Supplementary Information for
Theoretical model of efficient phagocytosis driven by curved membrane proteins and active cytoskeleton forces

Raj Kumar Sadhu[1*], Sarah R Barger[2], Samo Penič[3], Aleš Iglič[3], Mira Krendel[4], Nils C Gauthier[5], and Nir S Gov[1†]
[1]*Department of Chemical and Biological Physics, Weizmann Institute of Science, Rehovot 7610001, Israel*
[2]*Molecular, Cellular, Developmental Biology, Yale University, New Haven, USA*
[3]*Laboratory of Physics, Faculty of Electrical Engineering, University of Ljubljana, Ljubljana, Slovenia*
[4]*Department of Cell and Developmental Biology, State University of New York Upstate Medical University, Syracuse, USA and*
[5]*IFOM, FIRC Institute of Molecular Oncology, Milan, Italy*

This PDF file includes:

Supplementary Text

Secs. S1 to S16

Figs. S1 to S21

Legends for Movies S1 to S27

References (1 to 16)

Other Supplementary Materials for this manuscript include the following:

Movies S1 to S27

S-1. DISCRETE VERSION OF BENDING ENERGY

The bending energy of the vesicle has the form [1],

$$W_b = \frac{\kappa}{2}\int_A (C_1 + C_2 - C_0)^2 dA, \tag{S-1}$$

In the absence of any spontaneous curvature, the integration of the square of the mean curvature over the entire surface can be discretized in the following way [2]:

$$\int_A (C_1 + C_2)^2 dA = \sum_i \frac{1}{\sigma_i}\left[\sum_{j(i)} \frac{\sigma_{ij}}{d_{ij}}(\mathbf{R}_i - \mathbf{R}_j)\right]^2$$

where the outer sum runs over all the vertices and the inner sum runs over all the neighbours of i-th vertex. $\mathbf{R}_i$ is the radial vector of the vertex i, d_{ij} is the distance between the vertices i and j, σ_i is the area of the cell (formed by the vertex i and all its neighbours) in the dual lattice defined as,

$$\sigma_i = \frac{1}{4}\sum_{j(i)} \sigma_{ij} d_{ij}$$

* raj-kumar.sadhu@curie.fr
† nir.gov@weizmann.ac.il

where σ_{ij} is the distance between the vertices i and j in the dual lattice.

In the presence of curved membrane proteins, the spontaneous curvature of the i-the vertex is c_i (say). Then the bending energy of the i-th vertex can be written as,

$$W_b(i) = \frac{\kappa}{2}\sigma_i \left(\frac{h_i}{\sigma_i} - c_i\right)^2 \tag{S-2}$$

where,

$$h_i^2 = \left[\sum_{j(i)} \frac{\sigma_{ij}}{d_{ij}}(\mathbf{R}_i - \mathbf{R}_j)\right]^2$$

Thus, the total bending energy of the vesicle can be written as,

$$W_b = \sum_i W_b(i) \tag{S-3}$$

where, the sum runs over all the vertices of the vesicle.

S-2. CALCULATION OF A_{ad} AND A_{max} IN OUR SIMULATION

In our simulation, we define the adhesion energy (W_A) as the total number of adhered vertices multiplied by the adhesion strength E_{ad}. So, we do not actually calculate the true adhered area of the vesicle (A_{ad}), rather we only calculate the number of adhered vertices (N_{ad}) in our simulation. In order to estimate the adhered area from adhered number of vertices, we multiply the number of adhered vertices with the average area per vertex $< A > /N$, where $< A >$ is the average area of our vesicle (with fluctuations $< 1\%$ since the area is conserved in our simulation) and N is the total number of vertices in the vesicle. An estimation of $< A >$ can be made using the simplified assumption that the average area of a single triangle a_{av} is the area of the triangle when all its sides are of length $l_{av} = (l_{min} + l_{max})/2 = 1.35\ l_{min}$. This calculation gives $a_{av} \sim 0.79\ l_{min}^2$. The value of a_{av} calculated using our simulation gives $a_{av} \sim 0.76\ l_{min}^2$, which is very close to the above estimation. The total number of triangles in the vesicle are $\sim 2N$ for $N \gg 1$. So, the average area per vertex $< A > /N \sim 2a_{av}$.

In order to calculate A_{max} in the case of a full engulfment, we calculate the maximum number of adhered vertices N_{max}, and then multiply with the factor "adhered area per vertex". The maximum number of adhered vertices (N_{max}) in a full engulfment case may also vary slightly when we change any parameter such as E_{ad}, ρ etc. So, we scan the value of N_{max} for a given E_{ad} by changing other parameters, such as ρ, F etc., and consider the maximum one to be our N_{max}.

Since, in almost all cases, we are mainly interested in the ratio of A_{ad}/A_{max}, the factor for the "adhered area per vertex" cancels, and does not matter much, however, when we need to compare the actual adhered area with the surface area of the particle, we indeed need to estimate the adhered area by multiplying the adhered number of vertices with this factor.

Since we have a finite resolution above the surface area of the particle within which we assume the vertex to be adhered, and this resolution is assumed to be l_{min}, the maximum adhered area A_{max} for a fully engulfed case may in general be larger that the true surface area of the particle. The maximum and minimum bound in this area for a spherical particle can be given as, $4\pi R^2 \leq A_{max} \leq 4\pi(R+1)^2$. The maximum fluctuation can thus be estimated to be $\sim (2R+1)/R^2 \sim 20\%$ for the case when $R = 10\ l_{min}$. This fluctuation will be negligible for a very large particle ($R \gg 1$).

S-3. RESULTS FOR PROTEIN-FREE VESICLE

Here, we discuss the engulfment of spherical particles by a protein-free vesicle. In Fig. S-1a, we show the phase diagram in the $R - E_{ad}$ plane. The background color is showing the adhered fraction A_{ad}/A_{max}, where A_{ad} is the adhered area and A_{max} is the maximum adhered area. The value of A_{max} is in general larger than the surface area of the particle, since we have a finite width of adhesive interaction (l_{min}), within which the vesicle can fluctuate. This

value may also be different for different parameter regime, but the difference is almost negligible. In the calculation of adhered area fraction (background color of Fig. S-1a) we implement the following method: For a complete engulfment, we assume A_{max} to be the maximum adhered area for a given E_{ad} with different values of ρ, and divide all the adhered area by that value of A_{max} to get the adhered area fraction. For a partial engulfment, we choose the A_{max} corresponding to a higher E_{ad} closest to the original value of E_{ad}, for which we have a complete engulfment. We use similar methods for calculating the adhered area fraction for the passive and active cases as well.

We note that smaller particles are difficult to engulf, as the bending energy cost becomes higher than the adhesion energy gain (Movie-S2). So, in order to engulf a small particle, E_{ad} should be increased to large values. On the other hand, larger particle is engulfed at smaller E_{ad} (Movie-S1). Since the size of the vesicle is finite, a much larger particle will not be engulfed by the vesicle, rather the vesicle will spread over it. So, there is an optimal size of the particle, that requires the smaller E_{ad} to engulf. We consider this optimal radius to be $R = 10\ l_{min}$ and use this value in the main paper.

For a given values of E_{ad} we choose two particles with different sizes R, such that for one value, the engulfment is partial, while for the other value, the engulfment is complete. We then compare the adhesion energy gain and bending energy cost for both the cases in Fig. S-1(b). Similar to the previous cases (passive and active vesicle), here also, we can explain the engulfment process by the competition between adhesion and bending energy costs.

We also measure the engulfment time for a given $R(= 10\ l_{min})$ and for various E_{ad}. The engulfment time shows a divergence as we reach the critical E_{ad} (below which engulfment is incomplete) (Fig. S-1c). We also measure the curvature of the vesicle at the leading edge (rim) with the adhered fraction A_{ad}/A_{max} as the engulfment proceeds. We note that the curvature at the leading edge increases linearly with A_{ad}/A_{max} (Fig. S-1d). We use this linear behaviour of rim curvature in our analytical calculations.

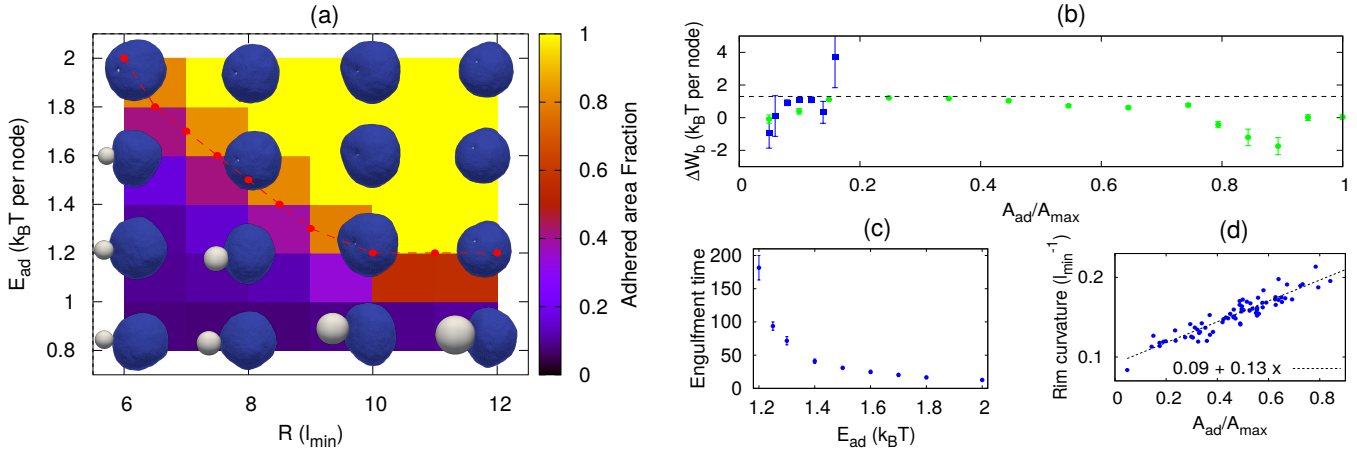

FIG. S-1: Engulfment of spherical particles by a protein-free vesicle. (a) Phase-diagram in the $R - E_{ad}$ plane. The background color is showing the adhered fraction. (b) Comparison of adhesion energy gain (E_{ad}, dashed horizontal line) and bending energy cost (W_b, points) (both in units of k_BT per adhered node) for partial and complete engulfment. Blue boxes are for $R = 8\ l_{min}$ and green circles are for $R = 10\ l_{min}$. We use $E_{ad} = 1.30\ k_BT$ here. (c) Engulfment time with E_{ad} showing divergence near the critical E_{ad} ($\sim 1.20\ k_BT$) below which there is no engulfment. Here, we use $R = 10\ l_{min}$. The unit of time is 5×10^5 M C steps. (d) Mean curvature at the rim (the leading edge of the vesicle) with adhered fraction A_{ad}/A_{max} for a complete engulfment. The parameters are same as in Fig. S-1b, green circles.

S-4. ANALYTICAL MODEL FOR PROTEIN-FREE VESICLE

Here, we present our simplified analytical (parametrical) model for protein free case. We consider a three-dimensional vesicle formed by a closed two-dimensional membrane, adhering to a spherical particle. We assume the system to be symmetric, such that we can only show a two-dimensional projection of the system on a plane (Fig. S-2). The vesicle area is $A = 4\pi R_0^2$, and the particle radius is R, such that $R < R_0$. As the vesicle engulfs the particle, the adhered fraction increases. The adhered area can be written as, $A_{ad} = 2\pi x R$, where x is the thickness of the spherical cap of the particle that is adhered, as shown in Fig. S-2. The leading edge of the membrane (rim) is highly curved, and the shape is assumed to be similar to a half-torus with one principal curvature $1/r$ and the other $1/h$. We assume $r \ll h$ and hence the other principal curvature is neglected. The area of this region can be written as $A_{rim} = 2\pi^2 r h$, where $h = \sqrt{2Rx - x^2}$.

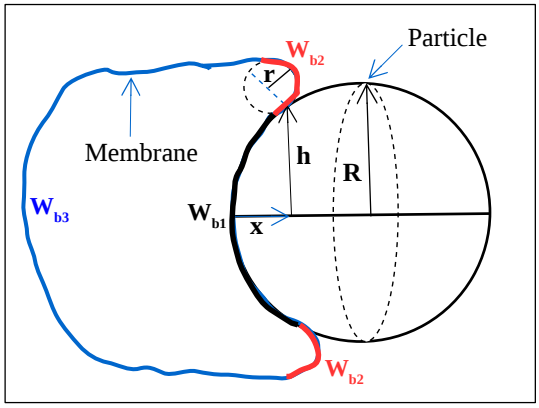

FIG. S-2: Schematic diagram of our analytical model. A spherical particle with radius R is being engulfed by a cell membrane of size R_0. We show the projection of the system on a plane. The bending energy contribution of the membrane can be divided by three parts: (1) The part of the membrane that is adhered to the particle, shown by black color (W_{b1}), (2) The part of the membrane that is unadhered and forming highly curved rim close to the particle, shown by red color (W_{b2}) and (3) The rest part of the membrane that is unadhered but having less curvature, shown by blue color (W_{b3}).

The bending energy of the adhered section of the membrane is,

$$W_{b1} = \frac{\kappa}{2} A_{ad} (2/R)^2 \tag{S-4}$$

and, the bending energy of the rim section is,

$$W_{b2} = \frac{\kappa}{2} A_{rim} (1/r)^2 \tag{S-5}$$

where, the mean curvature at the rim has the form, $1/2r = 1/R_0 + \alpha x/R$ (from simulation data in Fig. S-1d, where α is a fitting parameter), where α a constant and $A_{ad}/A \sim x/2R$, such that at $x = 0$, mean curvature becomes $1/R_0$, which is the mean curvature of the unadhered spherical vesicle.

We assume that the rest part of the unadhered vesicle have the same mean curvature as before, *i.e.*, $1/R_0$, thus, the bending energy of this section will be,

$$W_{b3} = \frac{\kappa}{2} (A - A_{rim} - A_{ad}) (2/R_0)^2 \tag{S-6}$$

The total bending is thus given as,

$$W_b = W_{b1} + W_{b2} + W_{b3} \tag{S-7}$$

We can now compare the adhesion energy gain and bending energy cost, as the engulfment proceeds, and can calculate the transition line.

A. Graphical solution for the transition line in the $R - E_{ad}$ plane

For a given value of E_{ad}, we plot the adhesion energy gain (E_{ad}) and the bending energy cost $\partial W_b/\partial A_{ad}$ with adhered area fraction, for few values of R (Fig. S-3). For very small R, the adhesion strength is not enough to overcome the bending energy cost and the particle will not be engulfed (Fig. S-3a). For a critical value of R, the adhesion strength will just be sufficient to overcome the bending energy cost, and the particle will be engulfed, as shown in Fig. S-3b. If we further increase R, the adhesion energy gain will be always higher than the bending energy cost, and the particle will easily be engulfed (Fig. S-3c).

We calculate the transition line by finding the line corresponding to E_{ad} which is just touching the peak of bending energy cost $\partial W_b/\partial A_{ad}$. We show this transition line in Fig. S-4, and also compare with the simulation line and the classical result from Ref. [3]. For the analytical model, we define E_{ad} as the adhesion energy per unit area, while in our simulation, we define it as the adhesion energy per vertex. While comparing the simulation and analytical results, we properly scale E_{ad} such that they become consistent with each other, s each vertex represents a patch of membrane of area $\sim 1.5 l_{min}^2$.

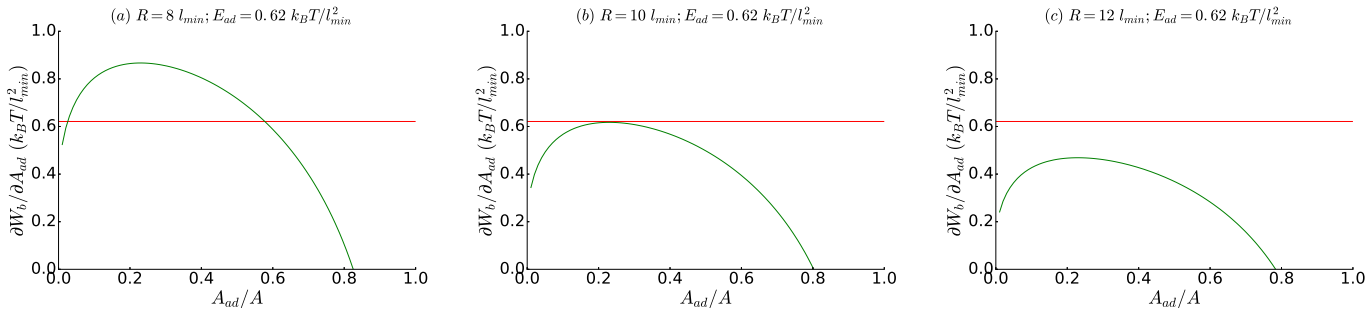

FIG. S-3: Comparison of adhesion energy gain (red line) and bending energy cost (green line) for few values of $R\ (= 8, 10, 12\ l_{min})$ and given $E_{ad} = 0.62\ k_BT/l^2_{min}$. Other parameters are, $R_0 = 20\ l_{min}$, $\alpha = 0.065$, $\kappa = 20\ k_BT$.

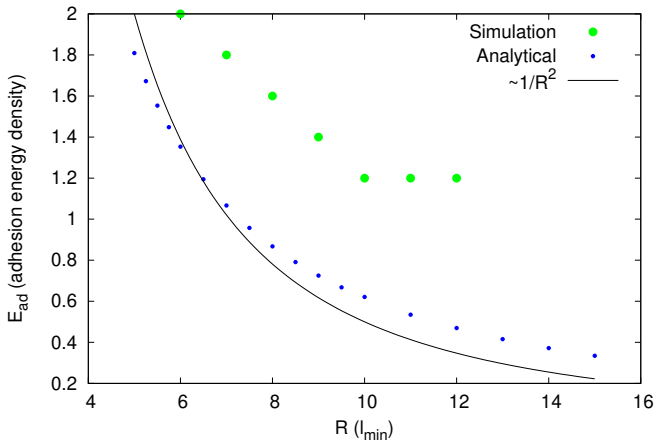

FIG. S-4: Transition line for engulfment in the $R - E_{ad}$ plane and comparison with simulations. In our analytical calculations, we define E_{ad} as the adhesion energy per unit area, while in simulation, we define it as the adhesion energy per adhered node. So, while comparing, we scale E_{ad} properly, so that the definition remains consistent with each other. The green circles are simulation result. The analytical prediction for the critical value of R with E_{ad} (blue circles), which is close to the classical prediction of $E_{ad} \sim 1/R^2$ [3], shown by black solid line. For simulation data, the parameters are same as in Fig. S-1a, and for analytical results, parameters are same as Fig. S-3.

S-5. RIM CURVATURE WITH ENGULFED AREA FRACTION FOR PASSIVE CASE

Here, we show that the mean curvature of the rim of the phagocytic cup varies non-monotonically with engulfed area fraction (Fig.S-5). It shows that the rim is energetically more favourable for the proteins around the peak value ($A_{ad}/A_{max} \sim 0.7$), Since there the bending energy is minimal: The bending energy depends on the mismatch between the mean curvature of the membrane and the spontaneous curvature of the proteins (Eq.S-1). The spontaneous curvature of the protein is $C_0 = 1l^{-1}_{min}$, so the bending energy is minimal when the mean curvature of the leading edge is maximal in Fig.S-5.

S-6. COMPARISON OF ADHESION AND BENDING ENERGY COSTS FOR PASSIVE PROTEINS WITH LARGE ρ

In Fig. S-6, we compare the adhesion and bending energy costs for the passive proteins with large ρ. Similar to the previous cases, we note that bending energy cost goes above the adhesion energy gain, just before complete engulfment, and the process stops with an incomplete engulfment.

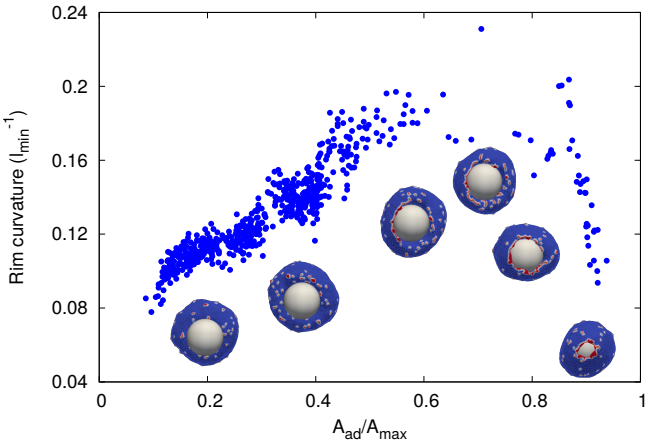

FIG. S-5: Rim curvature for the passive case with small protein density. We use here, $E_{ad} = 1.0\ k_BT$, $\rho = 3.2\%$.

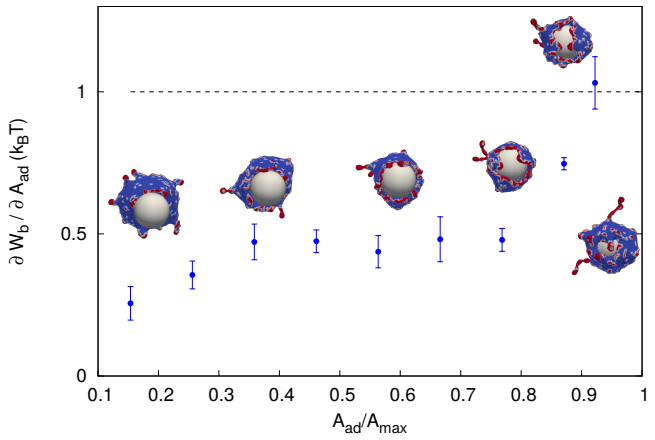

FIG. S-6: Comparison of adhesion and bending energy costs for passive proteins with large ρ. Here, we use $E_{ad} = 1.0\ k_BT$, and $\rho = 16.0\%$.

S-7. EXTENSION OF THE ANALYTICAL MODEL FOR PASSIVE CURVED (CONVEX) PROTEINS CASE

We here extend our analytical model for the passive curved protein case, with spontaneous curvature $c_0 = 1.0\ l_{min}^{-1}$. Let ρ_0 be the average protein density on the membrane, ρ_r be the density at the rim and ρ_s be the density on the rest of the unadhered part of the vesicle. We assume there are no proteins on the membrane that is adhered to the spherical substrate. Thus,

$$A\rho_0 = A_{rim}\rho_r + (A - A_{rim} - A_{ad})\rho_s \tag{S-8}$$

The bending energy of the adhered section is given by,

$$W_{b1} = \frac{\kappa}{2} A_{ad}(2/R)^2 \tag{S-9}$$

The bending energy of the rim is,

$$W_{b2} = \frac{\kappa}{2} A_{rim}(1/r - c_0\rho_r)^2 \tag{S-10}$$

where, the mean curvature at the rim, $1/2r = 1/R_0 + \alpha x/R$ and $\rho_r = \rho_0 + \beta x/R$ is the density at the rim (validated from simulation, Fig. S-7), where $\alpha = 0.093$ and $\beta = 0.085$ (determined from Fig. S-7). Assuming that the rest part of the unadhered vesicle have the same curvature of $1/R_0$, the bending energy of this part of the vesicle is given by,

$$W_{b3} = \frac{\kappa}{2}(A - A_{rim} - A_{ad})(2/R_0 - c_0\rho_s)^2 \tag{S-11}$$

Thus, the total bending energy cost is given by,

$$W_b = W_{b1} + W_{b2} + W_{b3} \tag{S-12}$$

A. Mean curvature and protein density at the rim (from simulation)

Here, we estimate the curvature and protein density at the rim of the phagocytic cup. In order to identify the rim of the phagocytic cup, we choose a region of the vesicle which is in between two concentric spheres of radius R and $R + R_c$, where R is the radius of the spherical particle that is being engulfed by the vesicle (see Fig. S-7a). We choose $R_c = 5\ l_{min}$ here. This methods works well as long as the region between the two radii does not cover a large portion of the vesicle, but is confined to the leading edge. At the latest stages of the engulfment this method is not very accurate as the region covers a large portion of the vesicle (see Fig.2c inset).

For the passive case with small protein density, we determine the mean curvature of the vesicle at the rim and plot it with adhered fraction of the particle, A_{ad}/A_{max} in Fig. S-7b. Similar to the protein-free case, here we note that the rim curvature seems to increase linearly, with a higher slope than the protein-free case. We also determine the protein density at the rim, and plot it with adhered fraction of the particle, A_{ad}/A_{max} (Fig. S-7c). The rim density also seems to vary linearly with the adhered fraction.

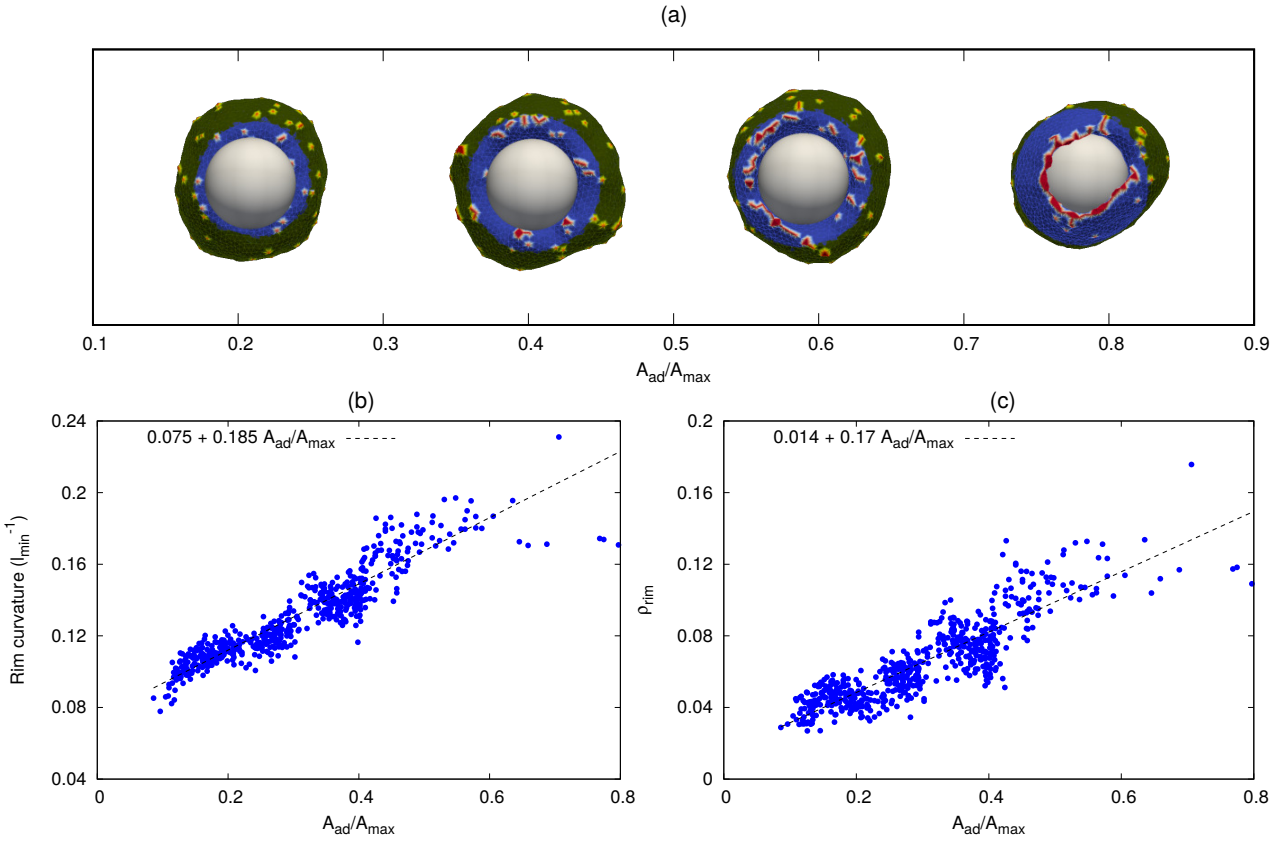

FIG. S-7: Mean curvature and protein density at the highly curved rim for passive case. (a) Scheme for the identification of rim of the phagocytic cup. The rim of the phagocytic cup is shown in usual color, while the rest part of the vesicle is shown in the green (unusual) color. (b) The mean curvature at the rim with adhered fraction of the particle A_{ad}/A_{max}. (c) The protein density at the rim with A_{ad}/A_{max}. The parameter used here are, $R = 10\ l_{min}$, $E_{ad} = 1.04\ k_BT$, and $\rho = 3.2$ %.

B. Graphical solution for the engulfment transition line in the $\rho - E_{ad}$ plane

Similar to the protein-free case, here also, we calculate the transition line in the $\rho - E_{ad}$ plane by using graphical method. We compare the adhesion energy gain and bending energy cost with adhered area fraction, for few values of protein density ρ and a given $R = 10\ l_{min}$ and given $E_{ad} = 0.39\ k_BT/l^2_{min}$ in Fig. S-8. For a small ρ, the vesicle will remain unadhered (Fig. S-8a). As we increase ρ, the adhesion energy gain will just become sufficient to overcome the bending energy cost, which is the transition value (Fig. S-8b). If we further increase ρ, the vesicle will be easily engulfed (Fig. S-8c), but for very high ρ the vesicle will not be fully engulfed rather will stop before full engulfment (Fig. S-8d). The analytic phase transition line is shown in Fig. S-9, compared to the simulation results (Fig. 1(a), main paper). The analytic model captures correctly the qualitative features of the engulfment transition line.

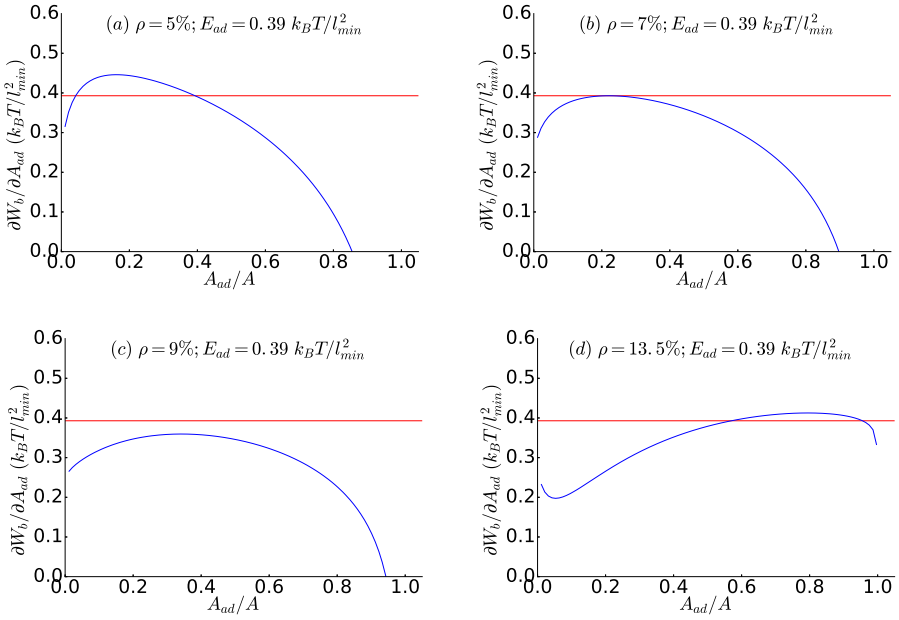

FIG. S-8: Comparison of adhesion energy gain (red line) and bending energy cost (blue line) for few values of ρ (= 5 %, 7 %, 9 %, 13.5 %) and given $E_{ad} = 0.39\ k_BT/l^2_{min}$. Other parameters are, $R = 10\ l_{min}$, $R_0 = 20\ l_{min}$, $\alpha = 0.093$, $\beta = 0.085$, $\kappa = 20\ k_BT$.

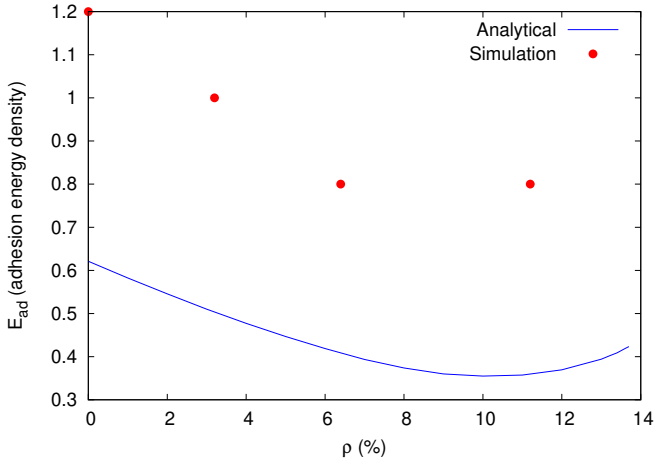

FIG. S-9: Transition line for engulfment in the $\rho - E_{ad}$ plane and comparison with simulations. The red circles are simulation result, and the blue line is the analytical prediction. For the simulation results, the parameters are the same as in Fig. 1(a) of the main text. For analytical results, parameters are the same as in Fig. S-8.

S-8. VARIATION OF ENGULFMENT TIME WITH ρ FOR PASSIVE CASE

We measure the engulfment time for a given E_{ad} and various values of ρ in Fig. S-10. We note that the engulfment time diverges as we reach the critical ρ (~ 2.25 %).

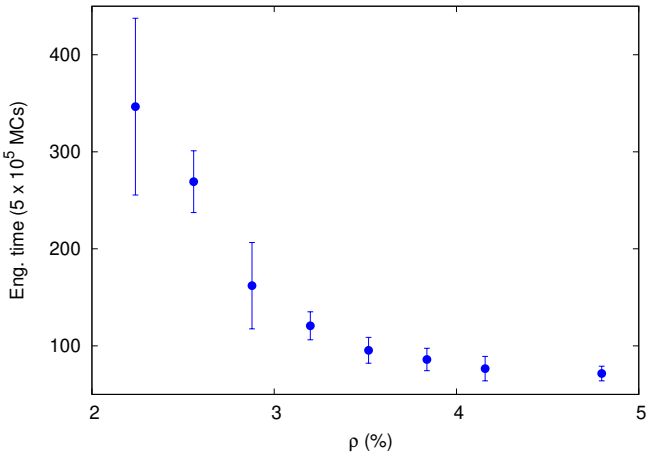

FIG. S-10: Engulfment time with ρ for passive case. The engulfment time diverges for critical $\rho \sim 2.25$ %, below which there is no engulfment. Here, we use $R = 10.0 l_{min}$ and $E_{ad} = 1.0\ k_BT$.

S-9. CALCULATION OF CONTRIBUTIONS DUE TO ACTIVE FORCES

In this section, we estimate the contribution of active forces in the engulfment process by calculating the work done by the active forces. Let us assume a force of magnitude F is acting on the membrane in the tangential direction of the surface of the particle (perpendicular direction of the radial vector of the particle) due to which the membrane extends to an infinitesimally small width dx (see Fig. S-11a). The circumferential length of the small extended strip $dl = 2\pi h$. Thus, the work done by the active force in this process is, $dW_F = Fdx$, and the increase in the adhered area $dA_{ad} = dx\ dl = 2\pi h dx$. Thus, the active energy gain, or the active energy per unit adhered area is given by,

$$\partial W_F / \partial A_{ad} = F/dl = F/2\pi h \tag{S-13}$$

In our simulation, we choose a region close to the spherical particle (the region in between two spheres of radius R and $R + R_c$, where we assume $R_c = 3\ l_{min}$), and assume that all the proteins inside this region is contributing in the engulfment process. We then calculate the component of force of all the proteins directed in the perpendicular direction of the radial vector of the particle, as shown by arrows in Fig. S-11b. The large arrow is showing the direction of net contribution. The rim length dl can be estimated from the adhered fraction of area, and thereby the contribution due to active forces can easily be estimated.

S-10. ENGULFMENT BY RAW 264.7 MACROPHAGES

Here, we show another dataset of the polystyrene particle engulfment by a RAW 264.7 macrophage using particle functionalized with immunoglobulin G (Fig. S-12).

S-11. CONFIGURATIONS FOR LARGE FORCE (F)

For a given E_{ad} and ρ, if we increase F to very large value, at some large value of F, the vesicle will deadhere from the particle, and will end up with no engulfment. In Fig. S-13a, we show such an example for $E_{ad} = 1.0\ k_BT$ and $F = 3.0\ k_BT/l_{min}$ for very small protein density ($= 1.6$ %). We note that vesicle gets deadhered from the surface of the particle with time, and finally ends up with no engulfment (Movie-S14).

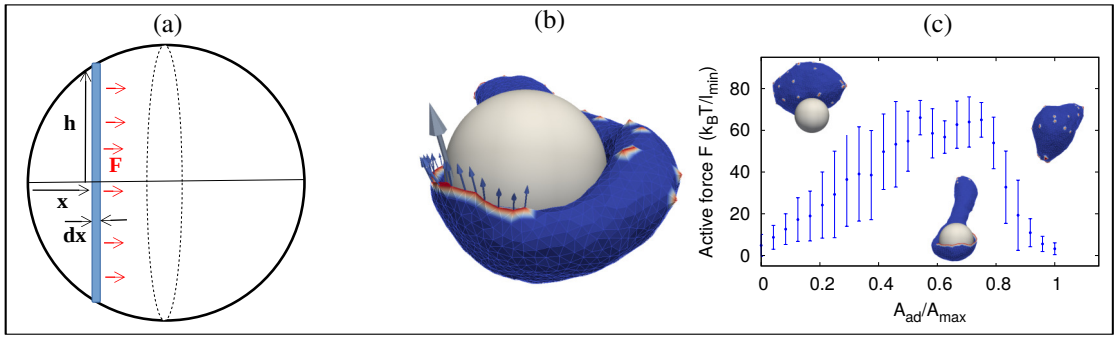

FIG. S-11: Calculation of contribution due to active forces in the engulfment process. (a) A schematic diagram for the calculation of active work done in the engulfment process. (b) A typical snapshot of vesicle engulfing a spherical particle forming an arc-like protrusion. The arrows are showing the direction of force which is perpendicular to the radial direction of the particle. The parameters used here are $E_{ad} = 1.0\ k_BT$, $\rho = 1.6$ % and $F = 2.0\ k_BT/l_{min}$.(c) Magnitude of total active force (along the tangential direction of the particle) with adhered fraction. Insets are showing the configurations corresponding to almost no engulfment, half engulfment and full engulfment cases. Parameters are same as in b.

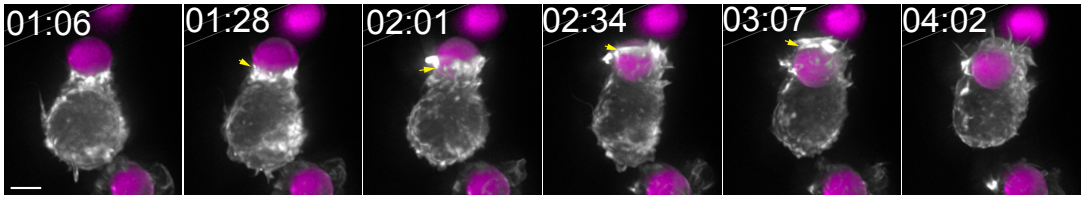

FIG. S-12: Engulfment of Immunoglobulin G-coated polystyrene particle by RAW 264.7 macrophage. Frames from a lattice light sheet movie (maximum intensity projections) of a cell transfected with mEmerald-Lifeact are shown. Time is indicated in min:sec, scale bar 5 μm

In the regime of large F, if we further increase ρ, a free vesicle (without adhesive spherical particle) can transform into a pancake-like shape [4]. In this regime, if we allow the vesicle to engulf the particle, it can engulf the particle if the force is not too large (Fig. S-13b). Since the engulfment process here is faster than the pancake transition process, the vesicle finally engulfs the particle before it transform into a pancake-like shape (Movie-S15). However, if we further increase F to even large value, we will again reach to a regime, where we do not have any engulfment (Fig. S-13c, Movie-S16).

S-12. REORIENTATION OF VESICLE WITH RESPECT TO NON-SPHERICAL PARTICLES OF HIGH ASPECT RATIO

In Fig. S-14a we show the reorientation process, first for a vesicle with passive curved proteins, that is initially in contact with a prolate particle from the top. Since, the top of a prolate shape with high aspect ratio is highly curved, the vesicle rotates and moves to the side of the particle, and finally engulfs it (Movie-S17). We quantify this rotation by the angular motion (θ) of the center of mass of the vesicle with respect to the particle (see S-14a, second inset). The angle becomes close to $\pi/2$ when the vesicle rotates completely from top to side, and then it engulfs the particle. The reorientation process in this case is fast, thereby, the total engulfment times for either top or side initial conditions are very similar (blue circles and red boxes in Fig. 5, main paper, for $R_x/R_z < 1$).

The reorientation of the vesicle from its initial position may not always be beneficial for engulfment. For an oblate particle with high aspect ratio, we note that the passive vesicle can engulf the particle from side quite easily (Fig. S-14b; Movie-S18). However, we frequently observed that an initial fluctuation caused the vesicle to slide over to the flat top regions, where it maximizes its adhesion energy at low bending cost. However, in this position the vesicle has to overcome a large bending energy barrier along the entire sharp equator of the oblate shape. For $R_x = R_y > 11\ l_{min}$ this barrier leads to no engulfment from the top orientation, and therefore reorienting to the top from the side will end up with no engulfment (Fig. S-14c; Movie-S19) [5]. In this case, we calculate the engulfment time by averaging only those realizations that end up with complete engulfment, while we discard the non-engulfed cases that shifted to the top position.

In Fig. S-14d we compare the bending energy cost and adhesion energy gain (E_{ad}, dashed line) per adhered node,

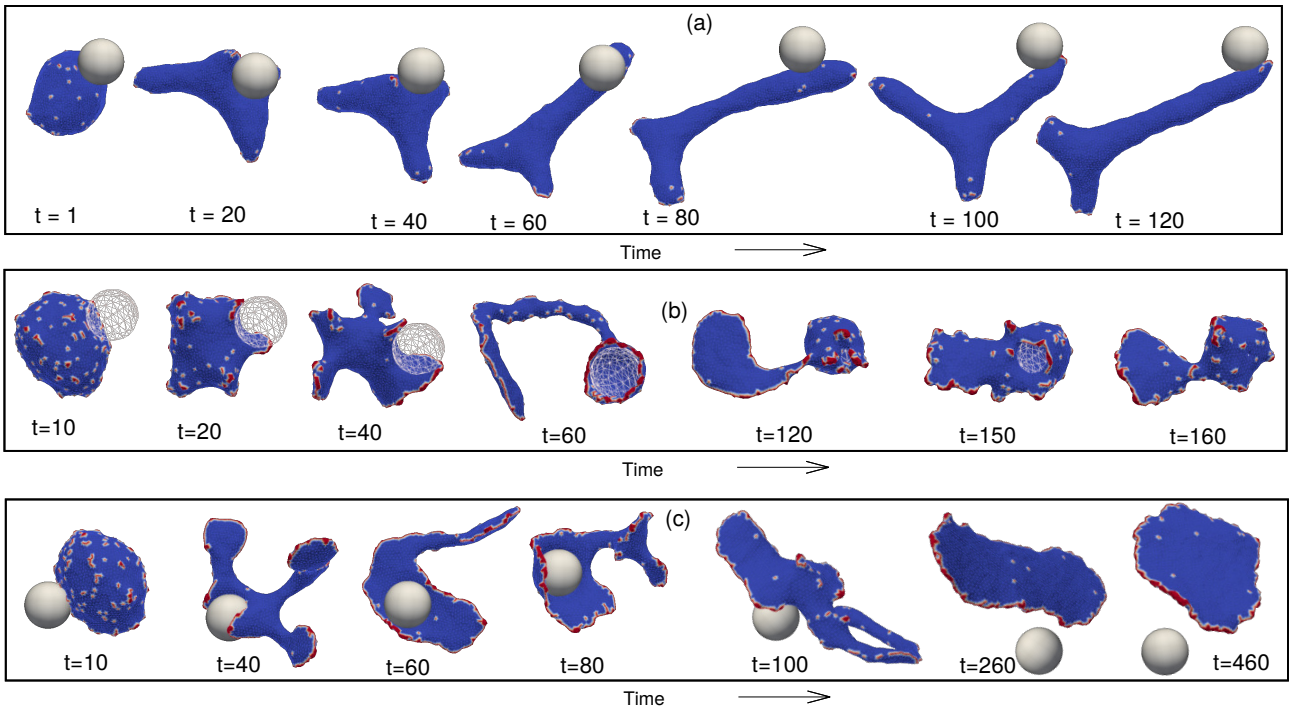

FIG. S-13: Engulfment of spherical particles by the vesicle with large force. (a) Configuration For very large force but small protein density. The engulfment becomes difficult and the particle ends up with no engulfment in this case. Here, we use $E_{ad} = 1.0\ k_BT$, $\rho = 1.6$ % and $F = 3.0\ k_BT/l_{min}$. (b) Configurations for a complete engulfment with very large ρ and F. Here, we use $E_{ad} = 1.0\ k_BT$, $\rho = 9.6$ % and $F = 3.50\ k_BT/l_{min}$. (c) Configurations for no engulfment with very large ρ and even larger F. Here, we use $E_{ad} = 1.0\ k_BT$, $\rho = 9.6$ % and $F = 4.0\ k_BT/l_{min}$.

for the vesicles with passive proteins of Fig. S-14(a-c). Similar to the engulfment of spheres (Fig. 1(b), main paper), we note that for the partial engulfment the bending energy cost increases above the adhesion strength, while for the complete engulfment the bending energy cost per node remains lower than E_{ad}.

For vesicles with active proteins we find similar reorientation of the vesicle with respect to its initial position on the particle. In Fig. S-14e we show such a case for a prolate particle with high aspect ratio. Similar to the passive case (Fig. S-14a), the vesicle rotates to the side, to avoid the highly curved pole, and then engulfs the particle from the side (Movie-S20). Since the active case is more dynamic, the vesicle sometime takes more time to reach the side orientation, and thereby the engulfment time is larger than when it is started from side. We also show similar observation for an oblate particle with high aspect ratio, where an active vesicle rotates from the side of an oblate particle to the top position (similar to the passive case Fig. S-14c) and then engulfs it (Fig. S-14f, Movie-S21). For an oblate shape, the engulfment is easier from the side (as shown for the passive case Fig. S-14b), but since the active vesicle is very dynamic, it does not engulf from side, but rather it reorients to the top in every realization and finally engulfs. This reorientation is however very fast, as the vesicle gains large adhesion energy in this process, thereby the engulfment time starting from either top or side are comparable (green circles and magenta boxes in Fig. 5, main paper, for $R_x/R_z > 1$).

We are therefore presented with a puzzle: what allows the active proteins to robustly engulf the oblate particle from the top orientation, whereas the passive vesicle faced a bending energy barrier that stalled the engulfment. This puzzle is further emphasized when we compare the bending energy cost and adhesion energy gain (E_{ad}) per adhered node, for both the prolate and oblate cases in Fig. S-14g. We note that for the oblate shape the bending energy cost can increase above the adhesion strength, as for the passive system (Fig. S-14d), but nevertheless the engulfment process does not stop. In this case, the active forces provide a mechanism to engulf the particle which we describe below.

For an oblate shape with high aspect ratios, we find that the active forces do not induce the formation of an arc-like aggregate of proteins at the rim of the phgocytic cup, as happens during the engulfment of the spherical particle

(Figs. 2(c-e), main paper). The active forces rather stretch the vesicle sideway, perpendicular to the particle surface, and this allows the stretched membrane afterwards to bend over the highly curved equator region of the oblate shape, leading to complete engulfment (Fig. S-14f). On the other hand, the passive vesicle is not stretched and remains spherical-like and fails to engulf the particle even for a much larger protein density (Movie-S22). This stretching of the vesicle by the active forces is quantified by measuring the volume of the vesicle, which becomes much lower than that of the passive vesicle as the adhered fraction increases (Fig. S-14h). We also show the cross-section view of both the passive and active vesicles for $A_{ad}/A_{max} \sim 0.45$ in the inset of Fig. S-14h, where the engulfment by the passive vesicle is stalled. Since the vesicle gets stretched for the active case, there is a significant bending energy contribution which arises far away from the surface of the particle, while for the passive vesicle the bending is dominated by the highly curved rim along the vesicle-particle leading edge (Fig. S-15). This indicates that the bending energy cost shown in Fig. S-14g also has a significant contribution due to a membrane that is far away from the particles, and is therefore not directly affected by the progression of the membrane-particle adhesion. The sideways stretching by the active forces is demonstrated by the force components plotted in Fig. S-14i. At the time where the vesicle is poised at the highly curved equator of the oblate shape, the vesicle is getting stretched by forces that are directed radially outward (F_r), while the engulfment is proceeding along the y direction. We note that the radial component F_r is much larger that the F_y component. We therefore identify here another mechanism by which active forces enable the engulfment to overcome bending energy barriers, which is qualitatively different from the mechanism described in Fig. 2, main paper. In Fig. S-16, we show some configurations close to the engulfment time to show how the stretching of the vesicle finally leads to full engulfment of the oblate particle.

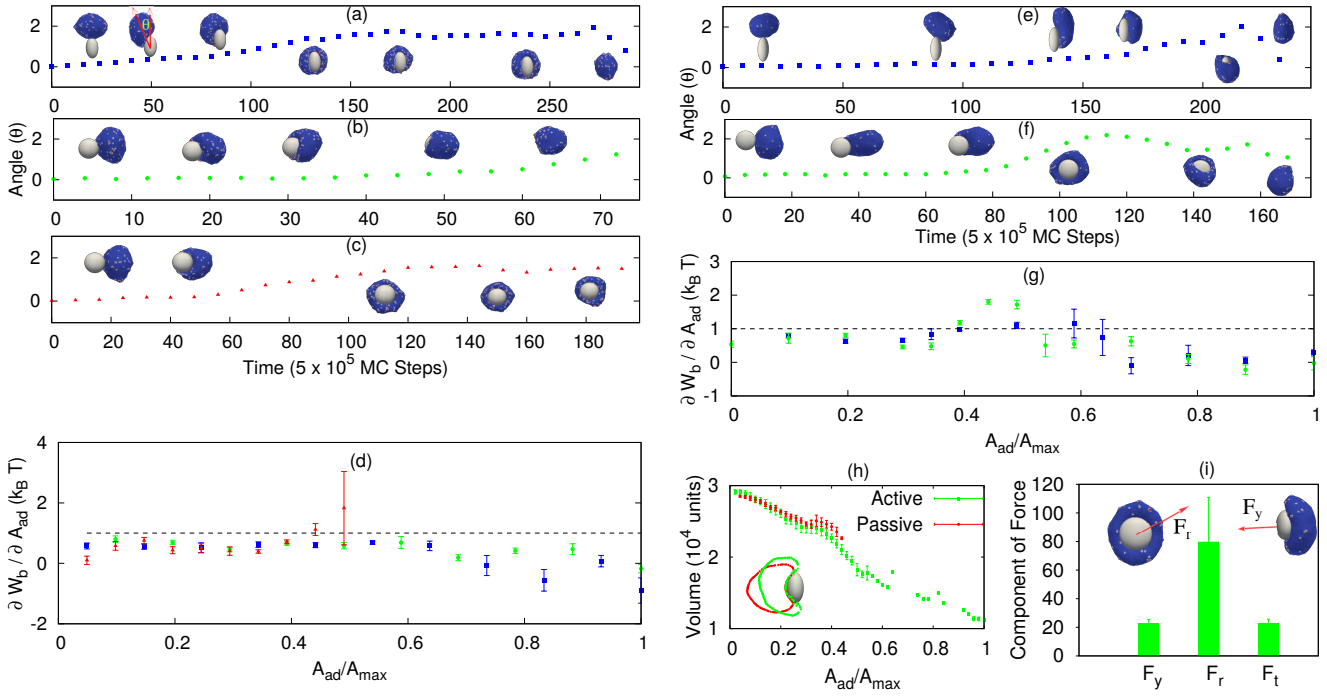

FIG. S-14: Reorientation of the vesicle with respect to its initial position on the surface of spheroid particles of high aspect ratio. The reorientation of the vesicle is quantified in (a-c) by the angular motion of the center of mass with respect to particle's surface (denoted in the inset of (a)). (a) A vesicle with passive proteins initiated from the top of a prolate spheroid, rotates over time, and finally completes the engulfment from the side. Here, we use $R_x = R_y = 8.4\ l_{min}$, $R_z = 14.16\ l_{min}$. (b-c) A passive vesicle is initiated from the side of an oblate shape and fully engulfs from side in (b), while it rotates to the top of the oblate shape and stalls around half-engulfment in (c). Here, we use $R_x = R_y = 11.4\ l_{min}$, $R_z = 7.96\ l_{min}$. (d) Comparison of bending energy cost $\partial W_b/\partial A_{ad}$ and adhesion gain (E_{ad}, dashed line) per adhered node (both having units of k_BT), for (a-c). (e) A vesicle with active curved proteins is initiated at the top of a prolate shape, rotates and engulfs from side. Here, we use $R_x = R_y = 7.6\ l_{min}$, $R_z = 16.29\ l_{min}$. (f) Active vesicle initiated at the side of an oblate shape finally engulfs from the top. Here, we use $R_x = R_y = 12.0\ l_{min}$, $R_z = 6.77\ l_{min}$. (g) Comparison of bending energy cost and adhesion gain (E_{ad}, dashed line) per adhered node, for (e-f). (h) Variation of the vesicle volume (in units of $10^4\ l_{min}^3$) for both active and passive proteins, initiated from the side of an oblate shape. The inset is showing the cross section of typical snapshots for both case for $A_{ad}/A_{max} \sim 0.45$. (i) Component of the active force along different direction for the active vesicle of (h), with $A_{ad}/A_{max} \sim 0.45$. For (h-i), we use $R_x = R_y = 12.0\ l_{min}$, $R_z = 6.77\ l_{min}$. For the passive case we use $\rho = 4.8$ % and for the active case, $\rho = 1.6$ %, $F = 1.0\ k_BT/l_{min}$. We used $E_{ad} = 1.0\ k_BT$ for all the plots.

A. Engulfment of oblate particles: Active vesicle shows high mean curvature far away from the particle

In Fig. S-14h, we compare the active and passive cases for the engulfment of an oblate particle with high aspect ratio, when the adhered area fraction $A_{ad}/A_{max} \sim 0.45$. Since the active vesicle gets stretched by the active forces, and thereby the bending energy cost will have dominant contribution far away from the surface of the particle. In order to quantify this, we measure the mean curvature of the vesicle section, which is having a perpendicular distance from the surface of the particle in between r and $r-1$ and plot it as a function of r for both the active and passive cases in Fig. S-15. As expected, the active vesicle have mean curvature larger than passive far away from the surface of the particle and it drops slowly with r. On the other hand, the passive vesicle has larger contribution only for small r and it drops faster with r.

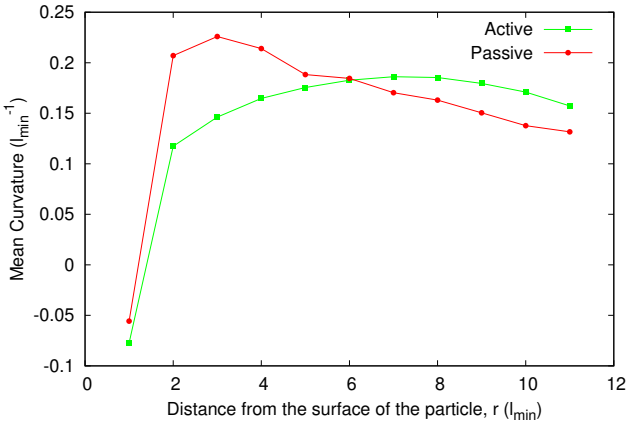

FIG. S-15: Mean curvature at a distance r from the surface of an oblate particle for $A_{ad}/A_{max} \sim 0.45$. Here, we use $R_x = R_y = 12.0\ l_{min}$, $R_z = 6.77\ l_{min}$ for the oblate particle. For passive case, we use $\rho = 4.8\%$. For active case, we use $\rho = 1.6$ % and $F = 1.0\ k_BT/l_{min}$. We use $E_{ad} = 1.0\ k_BT$ for both the cases.

B. Configurations for the engulfment of oblate shape by active vesicle close to the engulfment time

Here, we show the configurations for the engulfment of an oblate shape by an active vesicle, discussed in Fig. S-14(h-i). Here, we zoom into the time close to the engulfment to observe how the full engulfment proceeds.

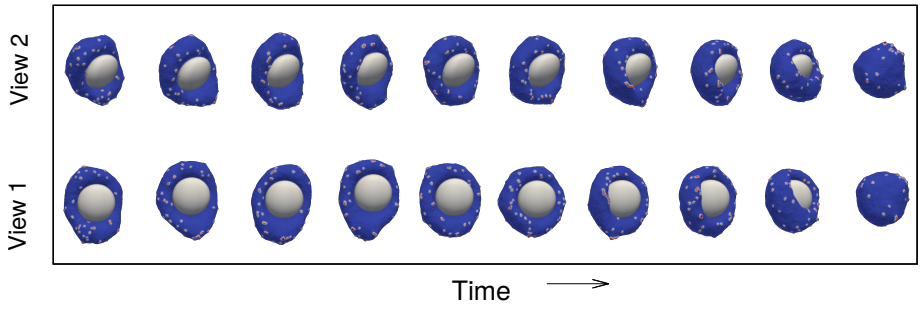

FIG. S-16: Configurations for the engulfment of an oblate by an active vesicle close to the engulfment time.

S-13. ENGULFMENT OF SPHERICAL PARTICLES WITH SMALLER RADIUS AND COMPARE WITH PROLATE/OBLATE PARTICLES

Here we simulate the engulfment of spherical particles with smaller radius, and compare with the maximum curvature of the prolate or oblate shape. For a prolate shape, the maximum mean curvature can be given by,

$$C_{max}(prolate) = \frac{1}{2}\left(\frac{R_z}{R_x^2} + \frac{R_z}{R_x^2}\right) \tag{S-14}$$

or, the radius of curvature corresponding to the maximal curvature is,

$$R_{min}(prolate) = \frac{R_x^2}{R_z} \tag{S-15}$$

Similarly, for an oblate shape,

$$C_{max}(oblate) = \frac{1}{2}\left(\frac{1}{R_x} + \frac{R_x}{R_z^2}\right) \tag{S-16}$$

and, the radius of curvature corresponding to the maximal curvature is,

$$R_{min}(prolate) = \frac{2R_xR_z^2}{R_x^2 + R_z^2} \tag{S-17}$$

From our simulation, we find that the smallest spherical particle that a vesicle with passive proteins can engulf, has a radius of $R \sim 8.5\ l_{min}$, while for a vesicle with active proteins, this minimal radius is: $R \sim 7.5\ l_{min}$ (Fig. S-17a). A sphere of radius $R = 7.5\ l_{min}$ will correspond to a prolate shape with maximum curvature (at its pole or top), given by $R_x = R_y \sim 9.4\ l_{min}$, $R_z \sim 11.63\ l_{min}$, and an oblate with maximum curvature (at its equator or side), given by $R_x = R_y \sim 11.4\ l_{min}$, $R_z \sim 7.96\ l_{min}$. Similarly, the sphere of radius $R = 8.5\ l_{min}$ will correspond to a prolate with $R_x = R_y \sim 9.65\ l_{min}$, $R_z \sim 10.98\ l_{min}$ and an oblate with with $R_x = R_y \sim 10.95\ l_{min}$, $R_z \sim 8.74\ l_{min}$. We show these co-ordinates in Fig. S-17b. The green dashed lines correspond to a local radius of curvature $R \sim 7.5\ l_{min}$ and the red dashed lines correspond to $R \sim 8.5\ l_{min}$. The good agreement between oblate shape of maximal aspect ratio that can still be engulfed by the passive vesicle, and the dashed line corresponding to $R \sim 8.5\ l_{min}$, shows that in this case the engulfment is indeed determined by the bending energy barrier at the equator (side, blue triangles). For the prolate particles, the vesicle generally reorients and feels a much smaller curvature while engulfing the particle, thereby the dashed lines deviate from the maximal aspect ratio for engulfment obtained from the simulations.

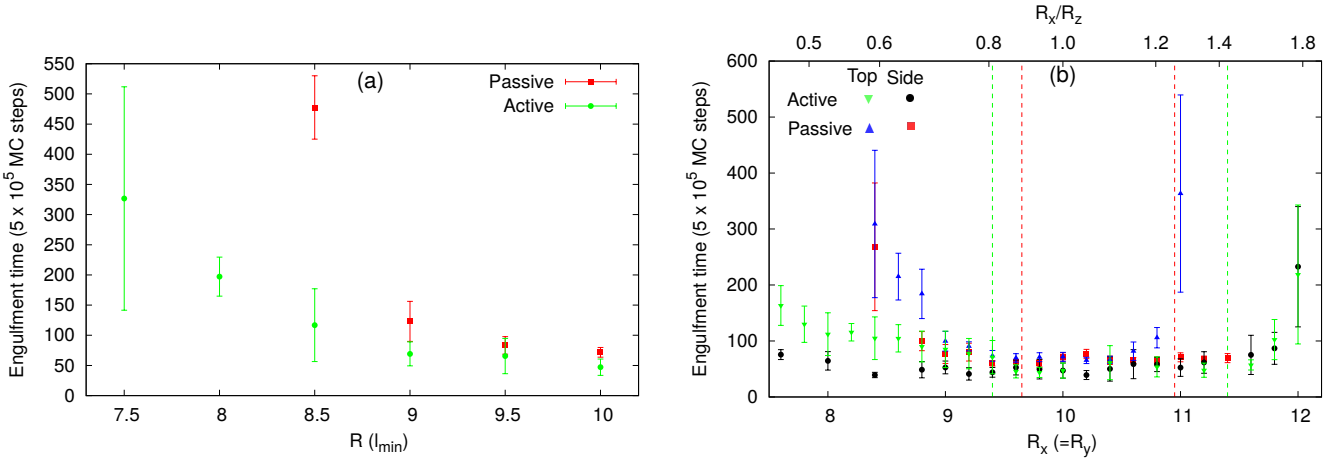

FIG. S-17: Engulfment of spherical particles with smaller radius, and comparison with prolate and oblate shapes. (a) The engulfment time as function of the radius R for a spherical particle. The engulfment time diverges as R decreases. (b) Comparison of the curvature of the spherical particle (below which engulfment time diverges, vertical dashed lines), with the maximum curvature of engulfed prolate/oblate particles (symbols, from simulations). The red dashed lines correspond to the sphere of radius $R = 8.5\ l_{min}$ (passive vesicle case) and the green dashed lines correspond to a sphere of radius $R = 7.5\ l_{min}$ (active vesicle case). Other simulation parameters are the same as in Fig. 5 of the main text.

S-14. ENGULFMENT OF BACTERIA-LIKE PARTICLES

Bacterial pathogens are often engulfed by phagocytic cells, as well as by cells which they invade [6]. We therefore investigate the engulfment of a sphero-cylindrical shape, resembling the shapes of different bacterias such as *E. coli* or *Bacillus subtilis* [7, 8]. This shape is an extreme case of a prolate spheroid, with an aspect ratio of 1 : 5. We use here a larger vesicle size ($N = 6127$), since the large aspect ratio of the particle requires a larger membrane area for engulfment.

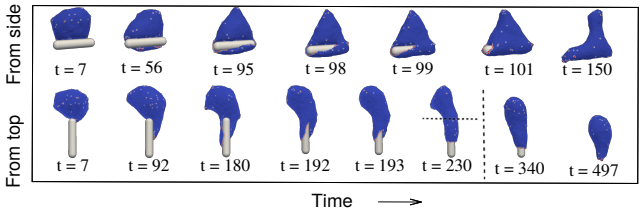

FIG. S-18: Engulfment of a sphero-cylindrical shape. The configurations are shown as function of the simulation time for a vesicle with active curved proteins, when initiated from the side (top panel), or from the top (bottom panel). The dashed vertical line in the lower panel shows the time at which we switch off the active forces of proteins that located above the horizontal dashed line shown for $t = 230$. The vesicle parameter values are $N = 6127$, $E_{ad} = 1.5\ k_BT$, $F = 1.5\ k_BT/l_{min}$, $\rho = 1.6$ %, while for the sphero-cylindrical shape: total length $l = 60\ l_{min}$ and radius $r = 6\ l_{min}$, such that the aspect ratio is 1 : 5.

When the initial contact between the vesicle and the particle is from the side, the engulfment proceeds smoothly (Fig. S-18, upper panel, Movie-S23). However, when initiated from the top, the initial engulfment stage is faster but later on the engulfment slows down and almost stalls (Fig. S-18, lower panel, before the dashed vertical line). This type of stalling is also observed in experiments [8]. In our simulations the stalling arises due to membrane tension, caused by active proteins that are located away from the engulfed article, and pull the membrane in the opposite the direction. We demonstrate this by turning off the active forces for all proteins that are located above the horizontal dashed line shown for $t = 230$, i.e. all the proteins that are on the opposite side of the phagocytic cup are made passive. The dashed vertical line in Fig. S-18 lower panel shows the time at which we turn off these active proteins, and we note that as a result the engulfment process proceeds quickly afterwards to completion (Movie-S27).

We can compare these simulation results to observed bacterial phagocytosis. In [7]. it was found that the velocity of engulfment was faster when the initial contact was from the pole of the bacteria. We find a similar behavior, as long as there is no restriction from membrane tension. Such tension can stall the engulfment in our simulations (Fig. S-18 lower panel), and indeed highly filamentous bacteria are found to avoid engulfment by immune cells [9], which we can attribute to the restriction of finite membrane area and the resulting membrane tension. The critical role of membrane tension during phagocytosis was previously shown experimentally [10].

We also explore the engulfment of dumb-bell like shapes, resembling the shape of fungi such as budding yeast [11]. A similar effect of membrane tension is also observed in our simulations during the engulfment such dumb-bell shaped particle (Fig. S-19, Movie-S25,S26). We found that while passive curved proteins can give rise to a smooth engulfment that does not stall (Fig. S-19a), the active vesicle can easily stall after engulfment of one lobe of the particle (i.e. when the leading edge is at the narrow neck) (Fig. S-19b). Releasing the membrane tension induced by the active proteins at the back of the vesicle, can release the vesicle and allow full engulfment. Similar hourglass shapes were previously shown theoretically to be susceptible to stalled engulfment [8], as well as in experiments observing phagocytosis of dividing yeast cells [11, 12] or highly deformable particles [13]. We also show the mean cluster size and the adhered fraction for both the passive and the active case in Fig. S-19(c-d).

S-15. RESULTS FOR MULTICOMPONENT MEMBRANE WITH PROTEINS OF DIFFERENT INTRINSIC CURVATURE

Here, we show our results for multicomponent membrane with proteins of different intrinsic curvature. We consider convex ($c_0 = 1.0\ l_{min}^{-1}$) as well as concave ($c_0 = -1.0\ l_{min}^{-1}$) proteins [14, 15]. We note that addition of concave proteins makes the engulfment easier in our model, in a parameter regime where only convex proteins fails to engulf the particle. This is somewhat similar to the engulfment process explored in [16], for membranes with uniform spontaneous curvature. In Fig. S-20, we show the engulfment by passive proteins with small E_{ad} ($= 0.80\ k_BT$) and convex protein density $\rho_p = 3.2$ % such that there is no engulfment, and compare with the case where in addition, we have concave proteins of density $\rho_n = 3.2$ %. The convex (concave) proteins have attractive interaction only with

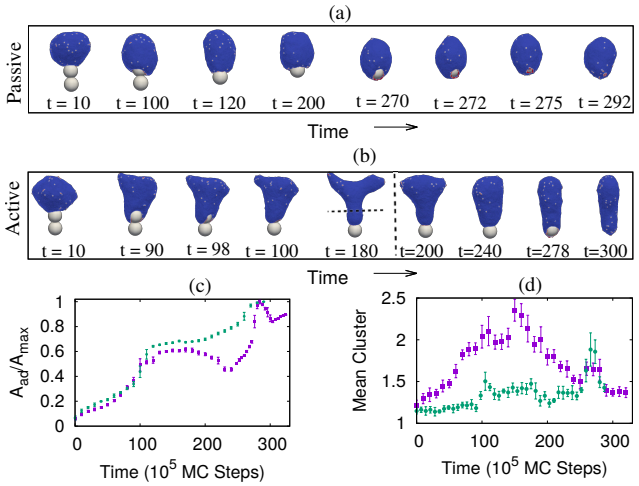

FIG. S-19: Engulfment of dumb-bell shaped particle. (a) Configurations with time for passive case. (b) Configurations with time for active case. The vertical dashed line is showing the time, when we remove the force from the proteins at the back. The horizontal dashed line on the configuration corresponding to $t = 180$ shows the coordinate above which we switch off the active forces of all the proteins. (c) Adhered area fraction with time. (d) Mean cluster size with time. Blue boxes are for active case and green circles are for passive case. The parameter values are $N = 6127$, $E_{ad} = 1.5\ k_BT$, $\rho = 1.6$ %. The radius of the spherical beads are 10 l_{min} each, and the overlapped region $l_p = 2\ l_{min}$, such that total length $L = 4R - l_p = 38\ l_{min}$. For active case, we use $F = 1.5\ k_BT/l_{min}$.

their convex (concave) neighbors. We note that the concave proteins aggregate close to the particle, and reduces the bending energy there. This allows the vesicle to adhere more and successfully engulf the particle (Movie-S24).

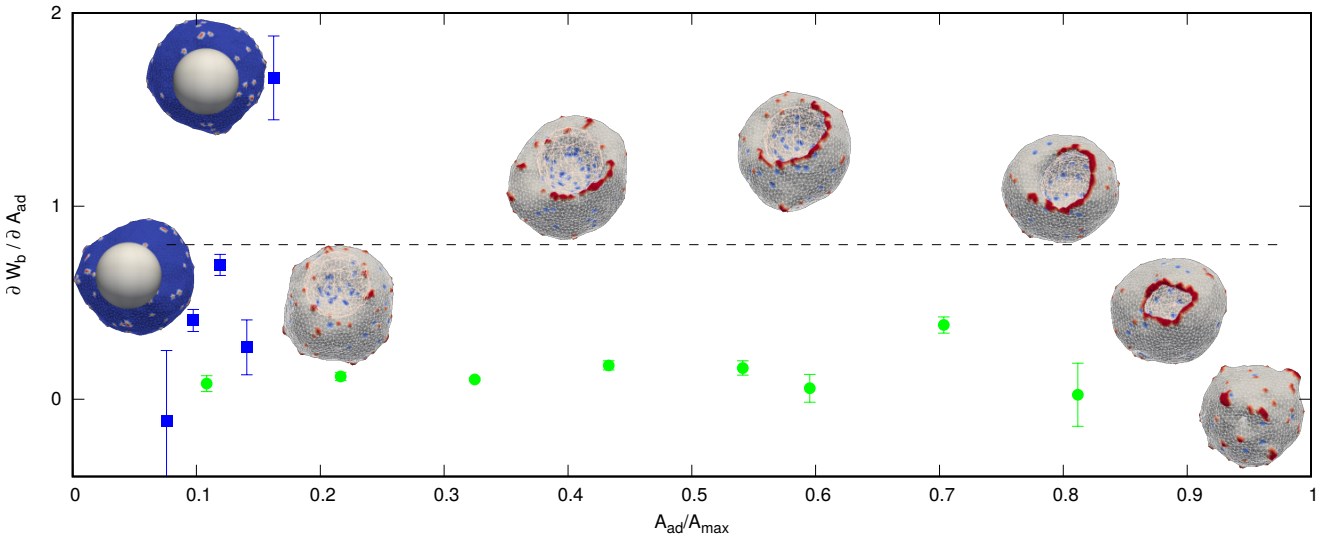

FIG. S-20: Results for multicomponent membrane with proteins of different intrinsic curvature. Here, we show the bending energy cost with adhered area fraction, and compare it with the adhesion strength E_{ad}. Blue boxes are for convex proteins, and green circles are for multiple proteins. Left insets are for convex proteins and right insets are for multiple curvature proteins. For multiple curvature case, red regions are denoting convex proteins, and blue regions are denoted concave proteins. Here, we use $R = 10.0\ l_{min}$, $E_{ad} = 0.80\ k_BT$, and $\rho_p = 3.2$ % for convex protein case. For multiple proteins case, we have in addition $\rho_n = 3.2$ %.

S-16. ERROR IN THE CALCULATION OF MEAN RADIUS OF CURVATURE

Here, we show the relative error (ΔR_c) in the calculation of mean radius of curvature of a vesicle without any proteins, compared to a spherical vesicle with same surface area (see Fig. S-21). We define this quantity as,

$$\Delta R_c = \frac{|R_c(triangulated) - R_c(spherical)|}{R_c(spherical)} \tag{S-18}$$

where, $R_c(triangulated)$ is the mean radius of curvature of a triangulated surface, and $R_c(spherical)$ is the mean radius of curvature of a spherical surface with same surface area as the triangulated surface. We find that the approximate description of the vesicle in terms of a triangulated network is very accurate for an average vesicle area of $\sim 5000\ l_{min}^2$, which is the typical size of the vesicle that we used in our simulations. The approximation of triangulation of the surface is reasonable even for a much smaller vesicle in our model ($< A > \sim 10\ l_{min}^2$), where the error is of order 10%.

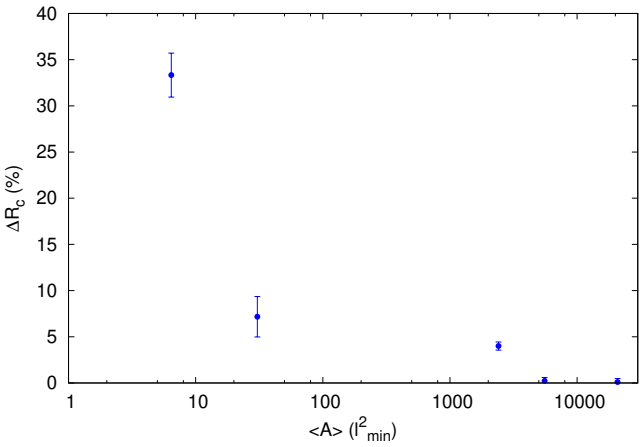

FIG. S-21: Relative error in the calculation of mean radius of curvature with total average area of a vesicle for protein-free case. The error is very small for a vesicle with area $\sim 5000\ l_{min}^2$, which is the typical vesicle size we use in our simulation.

Supplementary movies

High resolution supplementary movies are also available here.

- **Movie-S1** Complete engulfment of a spherical particle of larger radius by a protein-free vesicle. Here, we use $R = 10\ l_{min}$ and $E_{ad} = 1.30\ k_BT$.
- **Movie-S2** Partial engulfment of a spherical particle of smaller radius by a protein-free vesicle. We use here $R = 8\ l_{min}$ and $E_{ad} = 1.30\ k_BT$.
- **Movie-S3** Partial engulfment of a spherical particle by a passive vesicle with small protein density. We use $R = 10\ l_{min}$, $\rho = 2.4$ % and $E_{ad} = 1.0\ k_BT$.
- **Movie-S4** Complete engulfment of a spherical particle by a passive vesicle with medium protein density. Here, we use $R = 10\ l_{min}$, $\rho = 4.0$ % and $E_{ad} = 1.0\ k_BT$.
- **Movie-S5** Partial engulfment of a spherical particle by a passive vesicle with very high protein density. Here, we sue $R = 10\ l_{min}$, $\rho = 12.8\%$ and $E_{ad} = 1.0\ k_BT$.
- **Movie-S6** Partial engulfment of a spherical particle by an active vesicle with small force. The parameters are: $R = 10\ l_{min}$, $\rho = 1.6$ %, $E_{ad} = 1.0\ k_BT$ and $F = 0.10\ k_BT/l_{min}$.
- **Movie-S7** Complete engulfment of a spherical particle by an active vesicle with medium force. Here, we use $R = 10\ l_{min}$, $\rho = 1.6$ %, $E_{ad} = 1.0\ k_BT$ and $F = 0.40\ k_BT/l_{min}$.

- **Movie-S8** Complete engulfment of a spherical particle by an active vesicle with large force. We use here $R = 10\ l_{min}$, $\rho = 1.6$ %, $E_{ad} = 1.0\ k_BT$ and $F = 2.0\ k_BT/l_{min}$.

- **Movie-S9** Engulfment of spherical particle by an active vesicle with large ρ and small F. Here, we show fragmented protein clusters on the phagocytic cup at the early stage of engulfment. We use here $R = 10\ l_{min}$, $E_{ad} = 1.5\ k_BT$, $\rho = 6.4$ % and $F = 1.0\ k_BT/l_{min}$.

- **Movie-S10** Engulfment of spherical particle by an active vesicle with large ρ and large F. Here, we use $R = 10\ l_{min}$, $E_{ad} = 1.5\ k_BT$, $\rho = 4.8$ % and $F = 2.0\ k_BT/l_{min}$.

- **Movie-S11** Phagocytosis of Immunoglobulin-G-coated polystyrene bead (blue) by RAW264.7 macrophage transfected with mEmerald-Lifeact (orange). Maximum intensity projection of lattice light-sheet imaging. Scale bar, 5 μm. Time stamp: min:sec.

- **Movie-S12** Phagocytosis of Immunoglobulin-G-coated polystyrene bead (maroon) by murine bone-marrow derived macrophage transfected with mEmerald-Lifeact (gray). Maximum intensity projection of lattice light-sheet imaging. Scale bar, 5 μm. Time stamp: min:sec.

- **Movie-S13** Phagocytosis of Immunoglobulin-G-coated polystyrene bead (maroon) by RAW264.7 macrophage transfected with mEmerald-Lifeact (gray). Maximum intensity projection of lattice light-sheet imaging. Scale bar, 5 μm. Time stamp: min:sec.

- **Movie-S14** No engulfment of a spherical particle by an active vesicle with very large force. The movie shows a case, where particle is not engulfed by the active vesicle. Here, we use $R = 10\ l_{min}$, $\rho = 1.6$ %, $E_{ad} = 1.0\ k_BT$ and $F = 3.0\ k_BT/l_{min}$.

- **Movie-S15** Complete engulfment of a spherical particle by an active vesicle with very large force and large protein density. Here, we use $R = 10\ l_{min}$, $\rho = 9.6$ %, $E_{ad} = 1.0\ k_BT$ and $F = 3.50\ k_BT/l_{min}$.

- **Movie-S16** No engulfment of a spherical particle by an active vesicle with even larger force and large protein density. We use here $R = 10\ l_{min}$, $\rho = 9.6$ %, $E_{ad} = 1.0\ k_BT$ and $F = 4.0\ k_BT/l_{min}$.

- **Movie-S17** Complete engulfment of a prolate spheroid of high aspect ratio by a passive vesicle. The vesicle is initially started from the top and then rotates to the side and engulfs the particle. Here, we use $R_x = R_y = 8.4\ l_{min}$, $R_z = 14.16\ l_{min}$, $\rho = 4.8$ % and $E_{ad} = 1.0\ k_BT$.

- **Movie-S18** Complete engulfment of an oblate spheroid of high aspect ratio by a passive vesicle. The vesicle is initially started from the side, it engulfs the particle without reorienting itself to the other side. Here, we use $R_x = R_y = 11.4\ l_{min}$, $R_z = 7.96\ l_{min}$, $\rho = 4.8$ % and $E_{ad} = 1.0\ k_BT$.

- **Movie-S19** Partial engulfment of an oblate spheroid of high aspect ratio by a passive vesicle. The vesicle is initially started from the side, and it rotates to the top and ends up with no engulfment. The parameters are same as the previous movie.

- **Movie-S20** Complete engulfment of a prolate spheroid of high aspect ratio by an active vesicle. The vesicle is initially started from the top, and then reorients itself to the side and engulfs the particle. Here, we use $R_x = R_y = 8.4\ l_{min}$, $R_z = 14.16\ l_{min}$, $\rho = 1.6$ %, $E_{ad} = 1.0\ k_BT$ and $F = 1.0\ k_BT/l_{min}$.

- **Movie-S21** Complete engulfment of an oblate spheroid of high aspect ratio by an active vesicle. The vesicle is initially started from the side, and rotates to the top and engulfs the particle. Here, we use $R_x = R_y = 12.0\ l_{min}$, $R_z = 6.77\ l_{min}$, $\rho = 1.6$ %, $E_{ad} = 1.0\ k_BT$ and $F = 1.0\ k_BT/l_{min}$.

- **Movie-S22** Comparison of active and passive engulfment of an oblate shaped particle with high aspect ratio, initiated from side. For passive case the engulfment is partial while for active case, the engulfment is complete. Here, we use $R_x = R_y = 12.0\ l_{min}$, $R_z = 6.77\ l_{min}$, $E_{ad} = 1.0\ k_BT$. For active case we use $\rho = 1.6$ % and $F = 1.0\ k_BT/l_{min}$. For passive case, we use $\rho = 4.8$ %

- **Movie-S23** Engulfment of a sphero-cylinder by an active vesicle, when initiated from the top (from the spherical cap). Here, we use total number of vertices on the vesicle, $N = 6127$ radius of spherical cap $r = 6\ l_{min}$, total length $l = 60\ l_{min}$, $\rho = 1.6$ %, $E_{ad} = 1.50\ k_BT$ and $F = 1.50\ k_BT/l_{min}$.

- **Movie-S24** Engulfment of a sphero-cylinder by an active vesicle, when initiated from the side (from the cylindrical part). The parameters are same as the previous case.

- **Movie-S25** Engulfment of a dumb-bell shaped particle by a passive vesicle. Here, we use $N = 6127$ radius of spherical beads $R = 10\ l_{min}$, thickness of the overlapped region of the two beads $l_p = 2\ l_{min}$, $\rho = 1.6$ %, $E_{ad} = 1.50\ k_BT$.

- **Movie-S26** Engulfment of a dumb-bell shaped particle by an active vesicle. The movie shows the engulfment of a dumb-bell shaped particle by an active vesicle with $F = 1.50\ k_BT/l_{min}$. Other parameters are same as the previous case.

- **Movie-S27** Engulfment of a spherical particle by a passive vesicle with multiple curvature proteins. The movie shows a complete engulfment of spherical particle of radius $R = 10.0\ l_{min}$ by a passive vesicle, with $E_{ad} = 1.0\ k_BT$, convex protein density $\rho_p = 3.2$ % and concave protein density $\rho_n = 3.2$ %.

---

[1] W Helfrich. Elastic properties of lipid bilayers: Theory and possible experiments. *Zeitschrift für Naturforschung C*, 28(11-12):693–703, 1973.

[2] Domènec Espriu. Triangulated random surfaces. *Physics Letters B*, 194(2):271–276, 1987.

[3] R Lipowsky and H.-G Döbereiner. Vesicles in contact with nanoparticles and colloids. *Europhysics Letters (EPL)*, 43(2):219–225, jul 1998.

[4] Miha Fošnarič, Samo Penič, Aleš Iglič, Veronika Kralj-Iglič, Mitja Drab, and Nir S. Gov. Theoretical study of vesicle shapes driven by coupling curved proteins and active cytoskeletal forces. *Soft Matter*, 15:5319–5330, 2019.

[5] Jeroen S van Zon, George Tzircotis, Emmanuelle Caron, and Martin Howard. A mechanical bottleneck explains the variation in cup growth during fcγr phagocytosis. *Molecular Systems Biology*, 5(1):298, 2009.

[6] Klemens Rottner, Theresia E.B. Stradal, and Juergen Wehland. Bacteria-host-cell interactions at the plasma membrane: Stories on actin cytoskeleton subversion. *Developmental Cell*, 9(1):3–17, 2005.

[7] Jens Mölller, Tessa Luehmann, Heike Hall, and Viola Vogel. The race to the pole: how high-aspect ratio shape and heterogeneous environments limit phagocytosis of filamentous escherichia coli bacteria by macrophages. *Nano letters*, 12(6):2901–2905, 2012.

[8] David M. Richards and Robert G. Endres. Target shape dependence in a simple model of receptor-mediated endocytosis and phagocytosis. *Proceedings of the National Academy of Sciences*, 113(22):6113–6118, 2016.

[9] Akriti Prashar, Sonam Bhatia, Darren Gigliozzi, Tonya Martin, Carla Duncan, Cyril Guyard, and Mauricio R Terebiznik. Filamentous morphology of bacteria delays the timing of phagosome morphogenesis in macrophages. *Journal of Cell Biology*, 203(6):1081–1097, 2013.

[10] Thomas A Masters, Bruno Pontes, Virgile Viasnoff, You Li, and Nils C Gauthier. Plasma membrane tension orchestrates membrane trafficking, cytoskeletal remodeling, and biochemical signaling during phagocytosis. *Proceedings of the National Academy of Sciences*, 110(29):11875–11880, 2013.

[11] Margaret Clarke, Ulrike Engel, Jennifer Giorgione, Annette Müller-Taubenberger, Jana Prassler, Douwe Veltman, and Günther Gerisch. Curvature recognition and force generation in phagocytosis. *BMC Biology*, 8(1):154, Dec 2010.

[12] Régis Dieckmann, Yosuke von Heyden, Claudia Kistler, Navin Gopaldass, Stéphanie Hausherr, Scott William Crawley, Eva C Schwarz, Ralph P Diensthuber, Graham P Côté, Georgios Tsiavaliaris, et al. A myosin ik-abp1-pakb circuit acts as a switch to regulate phagocytosis efficiency. *Molecular biology of the cell*, 21(9):1505–1518, 2010.

[13] Daan Vorselen, Sarah R Barger, Yifan Wang, Wei Cai, Julie A Theriot, Nils C Gauthier, and Mira Krendel. Phagocytic 'teeth' and myosin-ii 'jaw' power target constriction during phagocytosis. *eLife*, 10:e68627, oct 2021.

[14] Kyoko Hanawa-Suetsugu, Yuzuru Itoh, Maisarah Ab Fatah, Tamako Nishimura, Kazuhiro Takemura, Kohei Takeshita, Satoru Kubota, Naoyuki Miyazaki, Wan Nurul Izzati Wan Mohamad Noor, Takehiko Inaba, Nhung Thi Hong Nguyen, Sayaka Hamada-Nakahara, Kayoko Oono-Yakura, Masashi Tachikawa, Kenji Iwasaki, Daisuke Kohda, Masaki Yamamoto, Akio Kitao, Atsushi Shimada, and Shiro Suetsugu. Phagocytosis is mediated by two-dimensional assemblies of the f-bar protein gas7. *Nature Communications*, 10(1):4763, Oct 2019.

[15] María José Sánchez-Barrena, Yvonne Vallis, Menna R. Clatworthy, Gary J. Doherty, Dmitry B. Veprintsev, Philip R. Evans, and Harvey T. McMahon. Bin2 is a membrane sculpting n-bar protein that influences leucocyte podosomes, motility and phagocytosis. *PLOS ONE*, 7(12):1–15, 12 2012.

[16] Jaime Agudo-Canalejo and Reinhard Lipowsky. Critical particle sizes for the engulfment of nanoparticles by membranes and vesicles with bilayer asymmetry. *ACS nano*, 9(4):3704–3720, 2015.